Work Project Report

Construction and performance study of the new Micro Pattern Gaseous Detectors for future upgrades of the CMS muon high rate region at the LHC

Francesco Fallavollita

July - August 2015

Main Supervisor
Prof. Cristina Riccardi

Second Supervisor
Prof. Sharma Archana

Index

1) Introduction

The *Compact Muon Solenoid* (*CMS*) detector is a general purpose detector operating at the *Large Hadron Collider* (*LHC*) at *CERN* to study proton-proton collisions. The following schedule is foreseen at the *LHC*: the collider has recently restart running and it will be working until 2018 (*Run 2*), it will be shut down from 2018 until the end of 2019 for *LS2* (*Long Shutdown 2*), will be running again from 2020 until the end of 2022 (*Run*3), will be shut down again in 2023-2025 (*LS3*) and restarted in 2025-2028 (*Run 4*). During *LS2* and *LS3* the *LHC* will be upgraded to achieve higher energy and luminosity (*Phase 1* and *Phase 2 Upgrades* respectively). After the *Phase 1 Upgrade* the luminosity will approach or exceed $2-3\times10^{34}\,cm^{-2}s^{-1}$, corresponding to $50-80$ interactions per crossing with $25\,ns$ bunch spacing operation. The CMS detector, including the muon spectrometer, is not capable of handling the higher data rates of the *LHC* expected in 2018 and beyond. In order to preserve an adequate detector performance and discovery potential in this high luminosity environment, significant detector improvements are required. One of the regions most severly affected by this luminosity improvement will be the high η region of the muon spectrometer, the region closest to the beam line. It will be characterized by high rates and high neutron and photon fluxes, making necessary the implementation of new detector based on innovative technologies capable of sustaining these harsh conditions. In particular, *GEM* (*Gas Electron Multiplier*) detectors have been selected for the *Muon System* and the study of their behavior in the expected environment is underway in order to increase their rate capability ($\sim MHz/mm^2$) and their radiation hardness ($20\,C/cm^2$) and simulations prove that an upgrade with *triple-GEMs* would bring significant improvements to the muon system's triggering and tracking capabilities. In addition, new detectors, like *Micro-Resistive WELL* detectors ($\mu-RWELL$ detectors) and *Fast Timing Micropattern* (FTM) detectors are currently under development and it will be of primary importance their comparison with the *GEM* detectors.

A *Gas Electron Multiplier* (*GEM*) detector consists of a thin-foil copper-insulator-copper sandwich chemically perforated to obtain a high density of holes, with a double-conical cross-section (hole diameter is typically between $25\,\mu m$ and $150\,\mu m$, pitch between $50\,\mu m$ and $200\,\mu m$). The central insulator is usually the polymer kapton, with a thickness of $50\,\mu m$. Application of a potential difference between the two sides of the *GEM* generates the electric field. Each hole acts as an independent proportional counter. The electrons released by the primary ionization particle in the upper drift region (above the *GEM foil*) are drawn into the holes, where charge multiplication occurs in the high electric field ($50-70\,kV/cm$). Most of avalanche electrons are transferred into the gap below the *GEM*. Several *GEM foils* can be placed at short distances (typically $1-2\,mm$) to distribute the gas amplification among several stages. A unique property of *GEM* detector is a full decoupling of the amplification stage (*GEM*) and the charge collection electrode-readout board of arbitrary pattern, placed below the last *GEM*. The signal detected on the *PCB* is generated only by the avalanche electrons (the ions do not contribute to the signal) and is typically a few tens of nanosecond for $1\,mm$-wide induction gap.

In the last years several new combinations of previous *MPGDs* have been built: the *WELL* detector, such as *Micro-Resistive WELL detectors* ($\mu-RWELL$ detectors) [4] and *Fast Timing Micropattern* (FTM) detectors [5], is realized by merging a suitable etched *GEM foil* with the readout *PCB* plane coated with a resistive deposition. The copper on the bottom side of the foil has been patterned in order to create small copper dots in correspondence of each *WELL* structure. The *WELL* matrix is hence realized on a thin kapton foil, copper-clad on both sides, with conical channels $70\,\mu m$ ($50\,\mu m$) top (bottom) diameter and $140\,\mu m$ pitch. A cathode electrode, defining the gas conversion/drift gap, completes the detector mechanics.

The main difference between a *GEM* and the *WELL detector* is that the *GEM* alone acts only as an amplifying stage and does not give positional information. To obtain such information, an extra plane of collection electrodes must be added to the detector, separated from the *GEM* by a distance of typically $1\,mm$ (in addition to the $3\,mm$ gas gap between the *GEM* and the drift window). It is clear that there is a big advantage in placing the read-out strips directly onto the kapton foil, as in the case of the *WELL detector*, eliminating the mechanical construction complications of an external, separate plane of electrodes. The resulting detector is extremely resistant to mechanical shock, overcoming the problems of fragility associated with chambers in which the electrodes are deposited on a thin glass substrate. Furthermore, it is desirable to keep the gas gap as thin as possible in order to work with a manageable high voltage on the drift. This requirement derives from the fact that the drift field of a gaseous detector, operated in the high magnetic fields of modern particle physics experiments, must be high enough to maintain a relatively small *Lorentz angle*. The *WELL detector* appear to overcome these problems [4, 6].

The limitation of most *MPGDs* comes from the fact that spark and discharge are easily formed inside the small amplification gap once heavily ionizing particles pass through them. The generation of the sparks in gas detectors is correlated with the transition from avalanche to streamer when the *Raether limit* is overcome, that is when the primary avalanche size exceeds $10^7 \div 10^8$ ion-electron pairs. Sparks may damage the detector and readout electronics and/or lead to large dead times as a result of HV breakdown. To decrease the spark probability, two or more *GEM foils* can be stacked one above the other, allowing to reach a higher gain and to decrease the spark probability of the structure for a given total gain. In particular *triple-GEM structures* seem very promising devices to be used at high luminosity colliders [7, 8]. With respect to a classical *single-GEM detector*, the *μ-RWELL detector* for example shows several advantages [6]:

1. small thickness (few millimeters) and very simple assembly procedure and then suitable for large area tracking devices as well as huge calorimetric apparata;

2. large gas gain: for prototypes studied, the maximum collection efficiency has been found in correspondence of a drift field of about $3.5\,kV/cm$ ($< 3.0\,kV/cm$ for the *single-GEM*). The maximum gain achievable with the μ-RWELL ($G \sim 6 \times 10^3\ at\ \Delta V \sim 525\,V$) is significantly higher than that one exhibited by a standard *single-GEM* used as reference ($G < 10^3\ at\ \Delta V = 500\,V$);

3. effective spark quenching: from a very qualitative analysis, the typical discharge amplitude for the *μ-RWELL* is of the order of few tens of nA (in any case less than $100\,nA$ also at the maximum gain), while for the *GEM* discharges with amplitude of the order of A are observed at high gas gain;

4. rate capability ranging for X-rays from $100\,kHz/cm^2$ to $600\,kHz/cm^2$ ($G \sim 2 \times 10^3$ and a surface resistivity of about $100\,M\Omega/\Box$).

2) Details of the Fast Timing Micropattern gaseous detector

The detector layout of the prototype is based on the concept of the *Micro-Resistive WELL detectors*: two layers are used for this first implementation, which is sketched in Figure 0.1. The multiplication volume is based on a pair of polyimide foils stacked due to the electrostatic force induced by the polarisation of the foils.

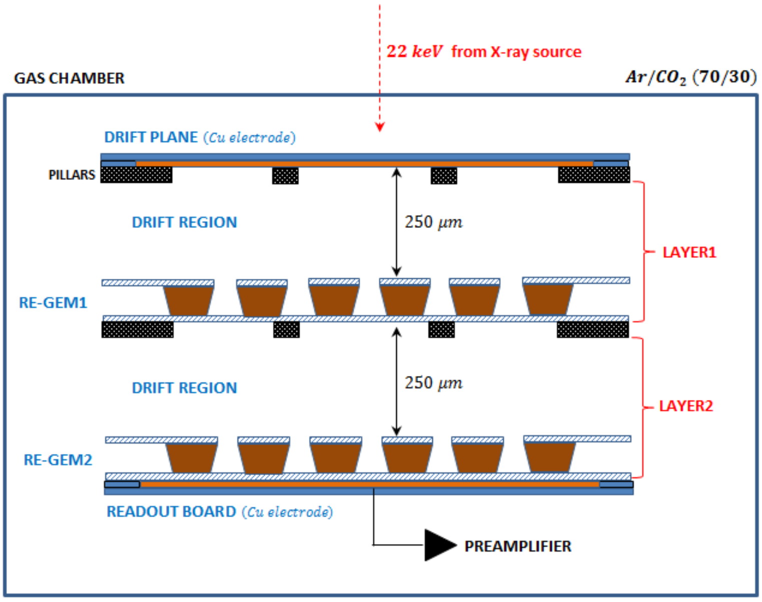

Figure 0.1: Schematic diagram of the first implementation of the FTM detector.

The perforated foils are a 50 μm thick Apical KANECA, which is initially coated with diamond-like carbon (DLC) techniques. This coating technique is used to provide, to the perforated polyimide foil, a potential gradient with resistive layers of the order of 800 $M\Omega/\square$, replacing the copper coating. The holes are inverted truncated cones with the two bases of 100 μm and 70 μm diameter. The pitch between holes is of 140 μm . The second foils are the 25 μm thick XC Dupont Kapton, which have a resistivity of the order of 2 $M\Omega/\square$. The drift volumes are 250 μm thick (see Figure 0.2).

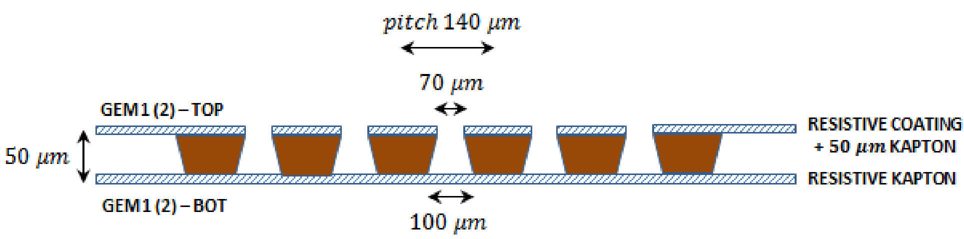

Figure 0.2: Schematic diagram of the perforated foils.

The planarity is ensured by a set of pillars obtained by PCB technique with photoimageable coverlay. The pillars' diameter is 400 μm with a pitch of 100 mm. The spacing around the active region is ensured by the use of two 125 μm-thick polyimide foils.

The employment of only resistive layers in the architecture allows signals coming from the layers to be externally extracted thanks to the resulting transparency of polarising electrodes. The prototype has been operated with $Ar/CO_2 = 70/30$ gas mixture. The different regions have been polarised with the *CAEN N1470* power supply in order to give an electric field of $2\,kV/cm$ for the drift regions and $100\,kV/cm$ for the amplification regions for an expected gain between 10^4 and 10^5. The signals from the Readout boar and Drift plane have been sent to the low-noise charge-sensitive *ORTEC PC142* preamplifier. The resulting inverted signal outputs have been amplified by the *ORTEC 474 NIM* module and acquired with a *Tektronix TDS 2024C* oscilloscope. An X-ray source has been used in order to demonstrated the capability of signal extraction, and the results are shown in Figure 0.3 where an average signal is shown in presence and absence of the source.

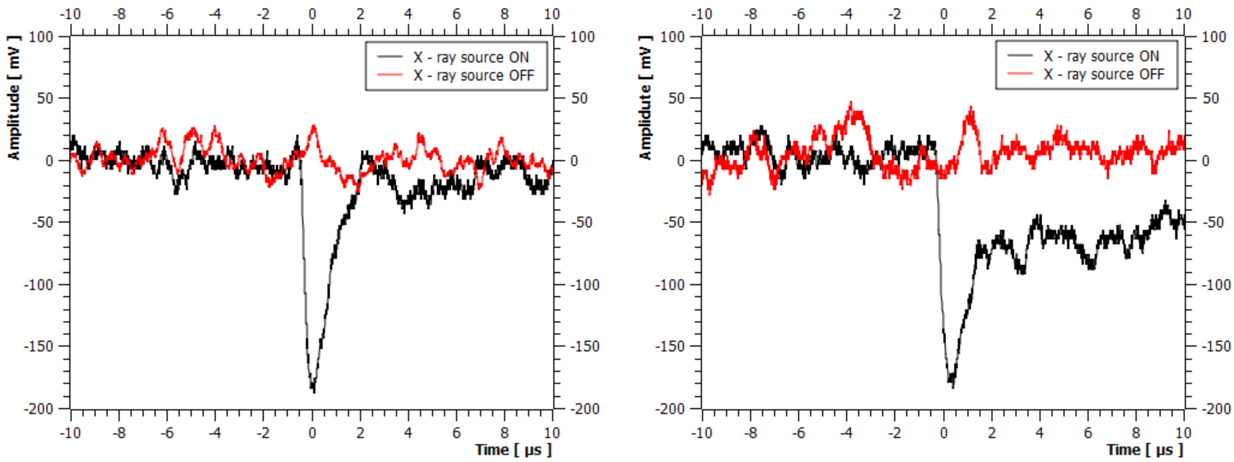

(a) (b)

Figure 0.3: Average FTM signal with X-ray source ON (black) and OFF (red). Signal read at the same time from Readout board (Figure a) and from Drift plane through capacitive coupling (Figure b) in order to demonstrated the transparency of the layers.

3) Result and interpretation

The *FTM* detector has been operated with $Ar/CO_2 = 70/30$ gas mixture and characterized by measuring the detector counting rate from Readout board and Drift plane in response to $22\,keV$ X-rays, generated by a *Mini-X* $50\,kV$ *Tube Amptek*, as a function of drift field for both layers (see Figure 0.1).

In a structure like the one discussed in this report (as well as for a GEM) some of the field lines in the conversion/drift region are expected to terminate on the resistive layer of the upper part of the amplification stage. Primary electrons following these lines are not collected into the WELL (hole) and therefore are not multiplied, producing a collection inefficiency. As shown in Figure 0.4-(a) the detector counting rate for a fixed value of the voltage applied to the WELL structure (i.e. for a fixed value of the amplification field), depends on the drift field. For the prototype studied in this work the maximum detector counting rate has been found in correspondence of a drift field of about $3.0\,kV/cm$ ($\sim 3.0\,kV/cm$ for the single-GEM).

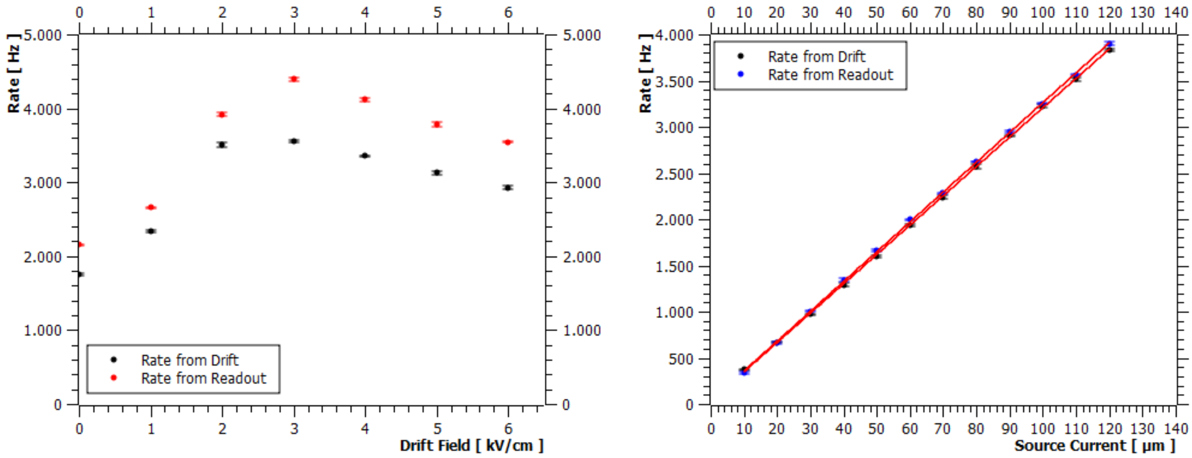

(a) (b)

Figure 0.4: In Figure (a) the detector counting rate from Readout board and Drift plane in response to $22\,keV$ X-rays as a function of drift field of *Layer-1* of the FTM prototype (see Figure 0.1) with a fixed value of the amplification field for both layers: $E_{Amp,Layer-1} = E_{Amp,Layer-2} = 110\,kV/cm$ and with a fixed value of the drift field of *Layer-2*: $E_{Drift,Layer-2} = 2\,kV/cm$. In Figure (b) the detector counting rate from Readout board and Drift plane as a function of collimated flux of $22\,keV$ X-rays with a fixed value of the drift and amplification field for both layers: $E_{Drift,Layer-1} = E_{Drift,Layer-2} = 2\,kV/cm$ and $E_{Amp,Layer-1} = E_{Amp,Layer-2} = 110\,kV/cm$. The same considerations made for *Layer-1* apply to *Layer-2* as well.

The detector counting rate from Readout board and Drift plane has been measured as a function of the collimated flux of $22\,keV$ X-rays, for both layers, changing the current of the X-Ray source. The results of this test are displayed in Figure 0.4-(b). The plot shows that no detectable drop in the detector counting rate from Readout board and Drift plane was observed over the full range of beam intensities.

The Signal to Noise Ratio (*SNR*) from Readout board and Drift plane for a single layer has been measured as a function of drift field. As shown in Figure 0.5 the Signal to Noise Ratio for a fixed value of the amplification field depends on the drift field.

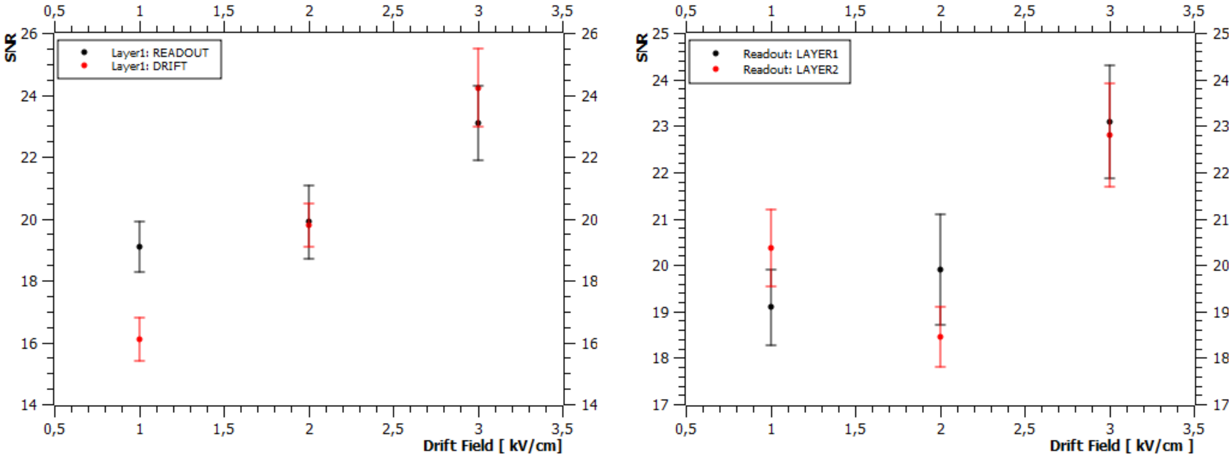

(a) (b)

Figure 0.5: In Figure (a) the *SNR* from Readout board and Drift plane in response to $22\,keV$ X-rays as a function of drift field of *Layer-1* with a fixed value of the amplification field: $E_{Amp,Layer-1} = 110\,kV/cm$. The same considerations made for *Layer-1* apply to *Layer-2* as well. In Figure (b) the comparison between *SNRs* from Readout board for *Layer-1* and *Layer-2* as a function of drift field with a fixed value of the amplification field: $E_{Amp,Layer-1} = 110\,kV/cm$.

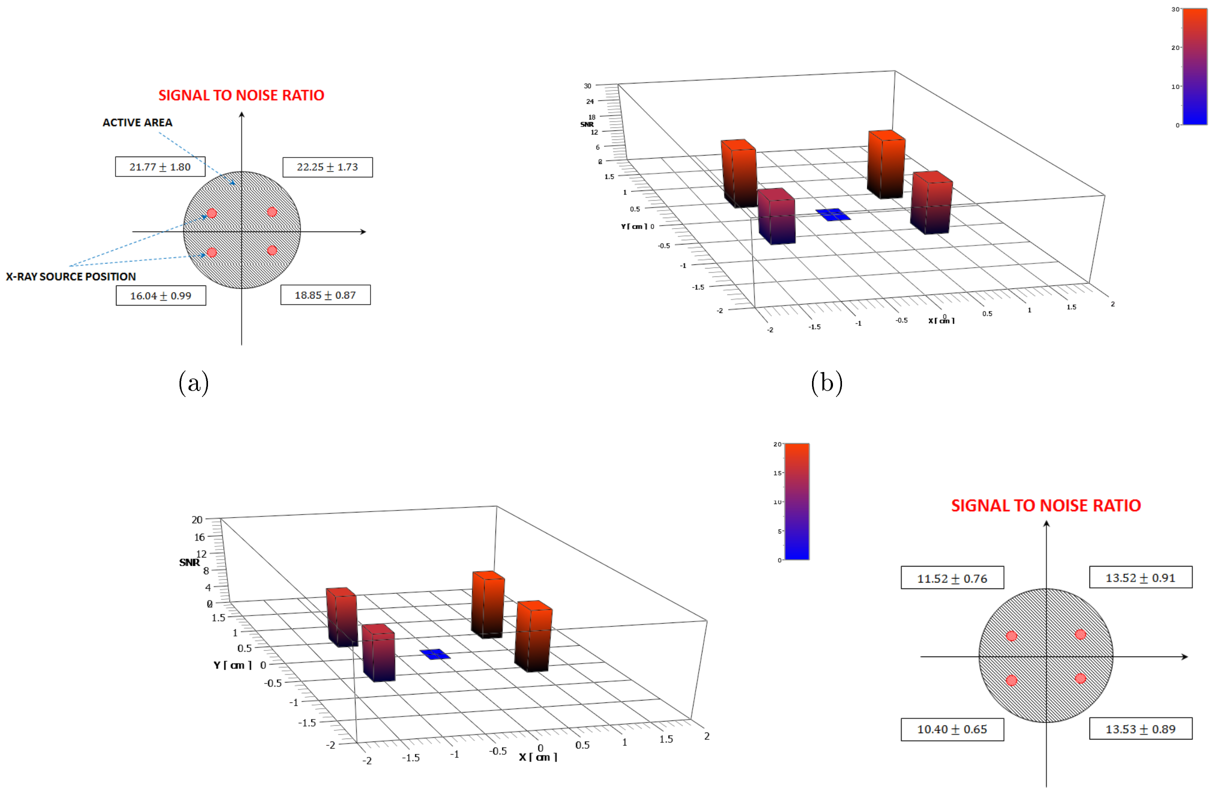

(a) (b) (c) (d)

Figure 0.6: In Figure (a) and/or (b) the Signal to Noise Ratio from Readout board and in Figure (c) and/or (d) the Signal to Noise Ratio from Drift plane for *Layer-1* as a function of the position of irradiation. The measurement has been performed with a drift field of around $2\,kV/cm$ and an amplification field of around $110\,kV/cm$.

The dependence of the Signal to Noise Ratio on the position of irradiation has been studied, using an $Ar/CO_2 = 70/30$ gas mixture, with a drift field of around $2\,kV/cm$ and an amplification field of around $110\,kV/cm$. Photons from our X-ray tube (Ag cathode, $22\,keV$) have been collimated to a spot of approximately $20\,mm^2$ and the remaining part of the active area of the detector has been shielded with a copper plate. The Signal to Noise Ratio has been measured as the beam was scanned along the middle of the sensitive area at four different position, as sketched in Figure 0.6-(a) or in Figure 0.6-(d) . For *Layer-1*, the Signal to Noise Ratio is plotted as a function of X-ray position in Figure 0.6-(b) for the Readout board and in Figure 0.6 (d) for the Drift plane. It can be seen that the Signal to Noise Ratio from the Readout board and the Drift plane for *Layer-1* is quite uniform over the four different measurement position.

4) Cosmic Stand

For future tests, a *Cosmic Stand* based on cosmic ray detection has been designed in its general geometrical structure in order to measure the efficiency and the timing resolution of the *FTM* prototype. As shown in Figure 0.7-(a), the *Cosmic Stand* is composed by a set of three scintillation detectors $10 \times 10\,cm^2$ (1) for the efficiency measurement, a set of three *Honeycomb GEM* $10 \times 10\,cm^2$ detectors (2) for the tracking performance and a device under test (i.e. the *FTM* prototype). The detectors are positioned on an appropriate mechanical structure and axially aligned at a distance of $15\,cm$ one from the other.

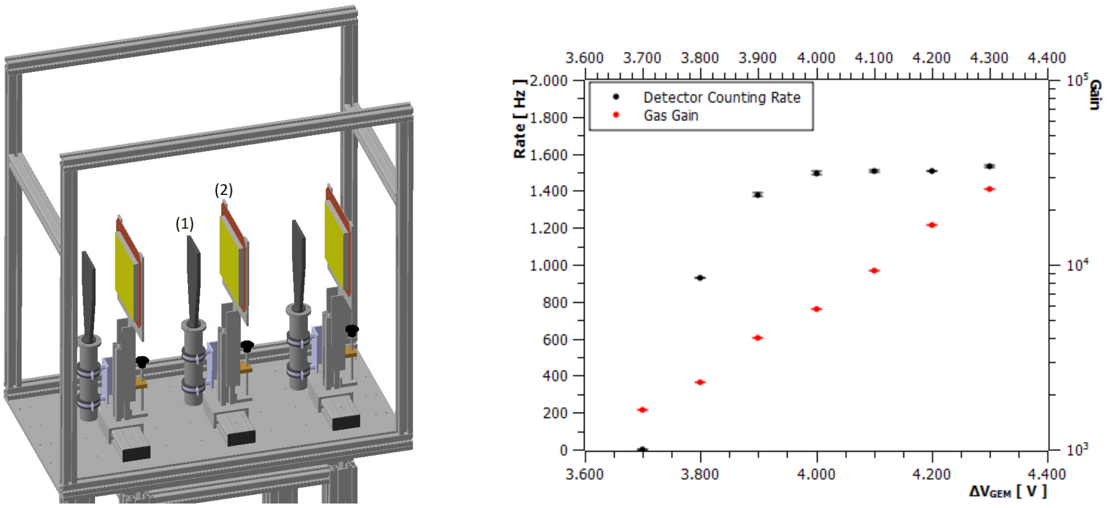

(a) (b)

Figure 0.7: In Figure (a) the schematic diagram of the *Cosmic Stand* in order to study the efficiency and tracking performance of the *FTM* detectors. In this picture the support for the *FTM* is still missing. In Figure (b) the detector counting rate (left ordinate) and gas gain (right ordinate) as a function of the potential applied with ^{55}Fe radioactive source.

The *GEM* detector has been operated with $Ar/CO_2 = 70/30$ gas mixture and characterized by measuring the detector counting rate and gas gain. The device has been irradiated with a collimated flux of 5.9 keV X-rays from a ^{55}Fe radioactive source. Some results of detector counting rate and gas gain vs. voltage measurements are presented in Figure 0.7-(b). The detector counting rate is an increasing function of ΔV_{GEM} and the detector starts to detect photons at a voltage as low as $\Delta V_{GEM} = 3700\,V$ that corresponds to an effective gas gain of about 1.6×10^3. A wide counting rate plateau is present between $4000\,V$ and $4300\,V$ and the working point of the detector is determined to be $4100\,V$. The gas gain has been measured as a function of the potential applied with a *Keithley-6485* pico-ammeter with 10 fA sensitivity. It is clear that the gain increases exponentially.

5) Conclusion

We have tested a new type position-sensitive gaseous proportional detector, called the *Fast Timing Micropattern* (*FTM*) detector, based on advanced printed circuit board technology, for fast timing applications. The construction feasibility has been demonstrated by building a first working prototype. We expect that this technique can be exploited for applications in high energy physics experiments, particularly for upgrades at *LHC* where sub nanosecond time resolutions are critical for particle identification and vertex separation. Other applications include X-ray diffraction studies and fast time-resolved measurements offer excellent medical imaging opportunities. In combination with an X-ray convertor and *FTM* and a visible photocathode shows great promise for use in digital mammography. Other applications include X-ray astronomy by exploiting time resolution of the *FTM* and selective sensitivity to soft X-rays.

Acknowledgements

The author is grateful to *Dr. I. Vai* for the continuous support and encouragement during the realization of this work. Moreover, he thanks *Dr. S. Salva* for her collaboration in the realization of this work and to *Dr. B. Dorney*, *Dr. J. Merlin* and *A. Puig-Baranac* to their support at the *Tracker Integration Facility - CERN*. He is grateful to *S. Franchino* for assembling the device and assisting with the measurements.

References

[1] F. Sauli, GEM: *A new concept for electron amplification in gas detectors*, Nucl. Instrum. Meth. A 386 (1997) 531;

[2] I. Giomataris et al., *Micromegas: a high-granularity, position sensitive gaseous detector for high particle flux environments*, Nucl. Instrum. Meth. A 376 (1996) 29;

[3] R. Bellazzini et al., *The Micro-Groove Detector*, Nucl. Instrum. Meth. A424 (1999) 444-458 INFN-PI-AE-98-02;

[4] R. Bellazzini et al., *The WELL detector*, Nucl. Instrum. Meth. A 423 (1999) 125-134;

[5] R. De Oliveira, M. Maggi, S. Archana, *A novel fast timing micropattern gaseous detector: FTM*, CERN-OPEN-2015-002 INFN-15-01/BA;

[6] G. Bencivenni et al, *The micro-Resistive WELL detector: a compact spark-protected single amplification-stage MPGD*, JINST, 10, (2015), P02008;

[7] F. Sauli, *Discharge studies and prevention in the gas electron multiplier*, CERN-EP/2000-151 (2000);

[8] M. Alfonsi et al., *High-rate particle triggering with triple-GEM detector*, Nucl. Instrum. Meth. A 518 (2004) 106;